Materials Characterization 214 (2024) 114082

Contents lists available at ScienceDirect

Materials Characterization

journal homepage: www.elsevier.com/locate/matchar

Investigating the flux pinning dependence on grain orientation in $YBa_2Cu_3O_{7-\delta}$ using neutron tomography

U.K. Oji [a,b,*], H. Fang [d], W. Ludwig [d,f], P. Lhuisser [c], Stavros Samothrakitis [e], Camilla Buhl Larsen [e], A. Hilger [b], I. Manke [b], M. Tovar [b], R. Cubitt [a], N. Kardjilov [b]

[a] Institut Laue-Langevin, Large Scale Structures Group, 71 avenue des Martyrs CS 20156, 38042 Grenoble, Cedex 9, France
[b] Helmholtz Zentrum Berlin für Materialen and Energie, D-14109 Berlin, Germany
[c] CNRS SIMaP, Grenoble-INP, Université Grenoble Alpes, Grenoble 38000, France
[d] European Synchrotron Radiation Facility, Grenoble 38043, Cedex 9, France
[e] Laboratory for Neutron Scattering and Imaging, Paul Scherrer Institut, CH-5232 Villigen PSI, Switzerland
[f] Université de Lyon, INSA Lyon, CNRS MATEIS, 69621 Villeurbanne, France

ARTICLE INFO

Keywords:
Superconductivity
Polarized neutron imaging
Magnetic structures

ABSTRACT

In this study, we report the first case of non-destructive characterization of the dependence of the flux trapping mechanism on the grain properties of a bulk type II superconductor using a combination of polarized neutron tomography and diffraction contrast tomography. The high temperature superconductor, $YBa_2Cu_3O_{7-\delta}$, has been used in this study due to its viable commercial growth processes typically resulting in the production of polycrystalline specimens. The diffraction tomography revealed the pseudo-single crystal nature of the sample i.e. a polycrystalline sample with 47 composite grains having a maximum grain misorientation angle of 1.86°. Polarized neutron tomography was used for characterization of the flux trapped in the material after field cooling to 90.5 K in a field of 0.5 mT and switching off the field. A combination of the results from these two non-destructive characterization techniques indicate a correlation between the anisotropy of the trapped flux with the orientation of the grains in the material in addition to a preference for the flux trapping in the grain boundaries.

1. Introduction

The discovery of High Temperature Superconductors (HTS) in the 1980s came with many predictions for potential applications. Given their relatively high transition temperatures (T_C) with some having T_C above the boiling point of Nitrogen, the cuprate superconductors showed the most promise in this respect. $YBa_2Cu_3O_{7-\delta}$ (YBCO) is a particularly prime candidate for use in applications due to its production cost advantage over other high temperatrure superconductors such as $Bi_2Sr_2Ca_2Cu_3O_x$ [1].

A complication arising with the use of cuprates such as YBCO in a majority of the applications is the requirement that the superconducting material should be able to sustain a significant amount of current during operation. While this is not a significant drawback for YBCO single crystals, which can be grown up to 7 cm with critical current density (J_C) values of up to 800 kA/cm^2 [2–4], YBCO grown via commercially viable processes such as hot-pressing typically have a polycrystalline nature. This polycrystalline nature could hinder the maximum attainable J_C in the material [5]. This limitation results mostly from the existence of grain boundaries which have been shown to be the significant detrimental factor to having maximum J_C in these materials. The IBM study of the effects of grain boundaries showed that, generally, their misalignment angle (θ_g) was a principle factor in determining the value of J_C with values of $\theta > 2$–3° leading to significant reductions of J_C [5]. Subsequent studies of the grain/grain boundary effects on J_C have shown that the value of J_C is not exclusively a function of θ_g. High values of J_C have been observed even in YBCO with high angle grain boundaries [6,7]. This has led to the discovery of the thermodynamic condition that affects the value of J_C which is the relation between the grain boundary energy and the surface energy [8]. The interplay between the grain boundary energy and the surface energy influences the grain boundary wetting ultimately determining the grain boundary's effect on the J_C value. Effectively, this means that J_C is not just a function of θ_g but also that of the 'cleanliness' of the grain boundaries.

* Corresponding author at: Institut Laue-Langevin, Large Scale Structures Group, 71 avenue des Martyrs CS 20156, 38042 Grenoble, Cedex 9, France.
E-mail address: u.oji@campus.tu-berlin.de (U.K. Oji).

https://doi.org/10.1016/j.matchar.2024.114082
Received 30 April 2024; Received in revised form 6 June 2024; Accepted 11 June 2024
Available online 18 June 2024

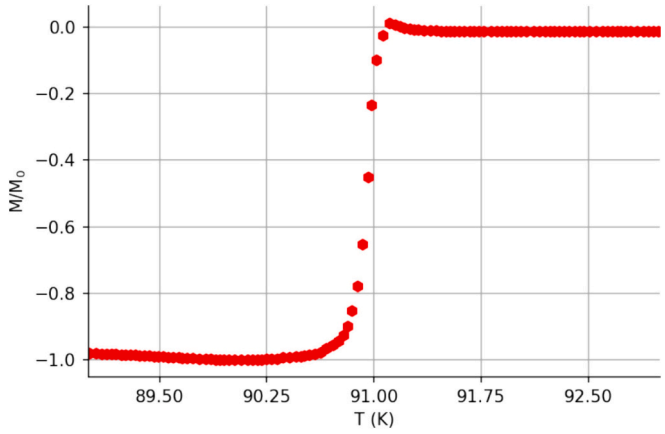

Fig. 1. Magnetization measured as a function of increasing temperature with an applied field of 0.07 mT. The 4 mm × 4 mm × 1 mm sample of $YBa_2Cu_3O_{7-\delta}$ stops being superconducting at $T = 91.3$ K.

Converse to the applications of HTS requiring a high J_C, their use in the production of superconducting quantum interference devices (SQUID) rely on these effects from the presence of grain boundaries that are considered detrimental to HTS in applications. The presence of the grain boundaries in the HTS facilitate the fabrication of Josephson Junctions [9,10] which are critical components of the SQUID sensor.

YBCO is known to have anisotropic properties resulting from both intrinsic and extrinsic features of the material such as the crystal structure and grain boundaries. The layered structure of the copper-oxide planes separated by insulating layers can result in an enhanced J_C due to its the intrinsic pinning when an external field, H//ab, is applied [11–13]. More pertinent to the work described in this paper, low angle grain boundaries create effective pinning centers for magnetic vortices via periodic dislocations arrays, leading to anisotropic flux pinning behavior [14–16] and ultimately contributing to the anisotropy of J_C in YBCO. It becomes clear that, regardless of the intended application for the HTS, an understanding of the flux pinning mechanism within grains and grain boundaries is imperative due to the dependence of J_C value on flux pinning in superconductors. In this paper, we present results from the study of grain/grain boundary effects on flux pinning in a bulk YBCO superconductor using neutrons. Specifically, neutron diffraction contrast tomography (DCT) has been used for reconstruction of the grains while polarized neutron tomography has been used to reconstruct the trapped field after field cooling in 0.5 mT and switching off the field. Neutrons are optimal for the non-destructive characterization of superconducting properties in bulk materials due to their combined superior penetration ability from their charge neutrality and their spin property. The results from the study suggest that, generally, the flux pinning has a directional dependence on the orientation of the grain/grain boundary. In addition, there is evidence suggesting a correlation between the magnitude of the pinned flux with the grain boundaries. These findings support, through visualization, the aforementioned flux trapping mechanism.

2. Experiment

2.1. Yttrium barium cuprate

A bulk ingot of $YBa_2Cu_3O_{7-\delta}$ is fabricated using standard top-seeded melt growth (TSMG) method. The sample is cut from this and has dimensions of 0.75 cm × 1 cm × 2.5 cm. YBCO typically has a superconducting transition temperature (T_c) of 91 K ± 1 [17]. Fig. 1 shows the sample temperature vs magnetization curve in 0.07 mT. From this, we can see that the sample stops being superconducting at 91.3 K as the temperature is increased. The transition is fairly sharp with ΔT <1 K. The sharpness of the transition can be an indication of the purity of the sample. High quality single crystals of YBCO have been shown to have transition widths of <1 K [18].

2.2. Neutron diffraction constrast tomography

2.2.1. Data acquisition

The DCT experiment was performed at the E11 beam-port of the BER II reactor of the Helmholtz-Zentrum Berlin, Germany and the basic setup is illustrated in Fig. 2. The Fast Acquisition Laue Camera for Neutrons (FALCON)21 [19] comprising of a forward and back-diffraction detector was used. Both detectors are made from ^{6}LiF- ZnS scintillator plates each with a total surface area of 412 × 412 mm^2 and a thickness of 210 μm. They are both coupled with four iCCD cameras of 2000 × 2000 total pixel area (206 μm pixel size). The sample-to-detector distances (L_{sd}) was 162 ± 2 mm for both detectors with a field-of-view of 412 × 412 mm^2 each giving an angular coverage of the diffracted neutrons using both detectors of more than 78% of 4π. The spatial resolution of the detectors was 600 μm. For the measurements, a continuous thermal neutron beam is used, utilizing the full available wavelength range of about 0.9 Å < λ < 3.2 Å. The sample has not been fully illuminated but done in heights of 3.3 mm for the 1 cm z dimension while the other dimensions have been fully illuminated being within the beam diameter of 5 mm. With an approximate 0.3° beam divergence, the diffraction data of all the grains constituting the sample height in the beam can be collected simultaneously. Diffraction data was acquired for multiple orientations of the sample with respect to rotation around a vertical axis, i.e. for a tomographic angle scan. Diffraction data has been collected over a rotation range of 320° with an angular step of 4°. This results in 81 projections with an exposure time of 60 s per projection.

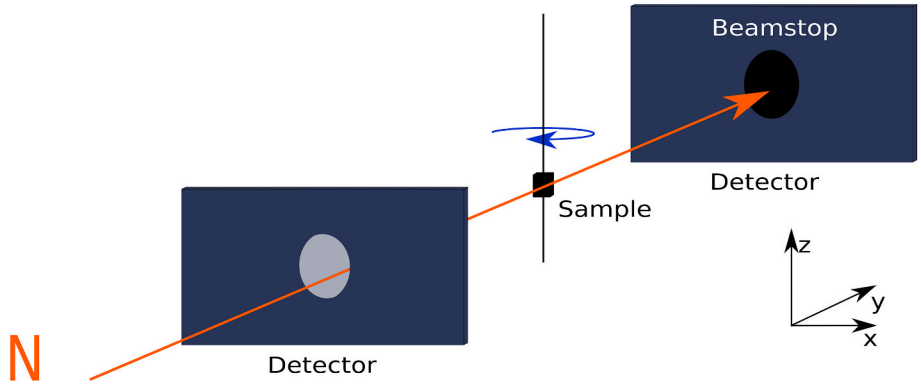

Fig. 2. Schematic of the Neutron Diffraction Computed Tomography experiment. The first detector is for backscattered neutrons while the second detector is for transmitted neutrons.

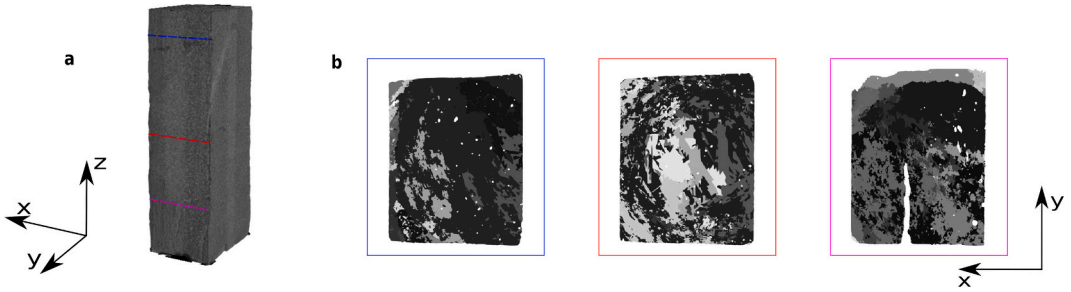

Fig. 3. (a) 3D tomographic volume of the YBCO sample with coloured dashed lines to indicate the investigated slices for each height stack in the experiment. (b) Selected x-y plane slices of the 3D reconstructed grains. The coloured boxes correspond to the position on the 3D volume with the same colour dotted lines.

2.2.2. Grain reconstruction

The reconstruction of the grain orientations and shapes, i.e. grain mapping, was performed using a forward projection based method developed by Fang and coworkers [20]. The core principle of this method is to index a sample voxel by maximizing its completeness, i.e. number of intersected spots between the forward calculation and experiment observation divided by the number of theoretically expected spots on the detector, and grow a region around the indexed voxel. The original reconstruction code is publicly available at [21]. Whilst this method was primarily developed for grain mapping by lab-based X-ray diffraction contrast tomography, it was flexible to be extended and adapted to the white neutron beam here.

To reconstruct grain maps, a tomographic volume reconstructed from a neutron absorption contrast tomography was segmented from pores/cracks to provide a volume mask for determining where to reconstruct the grains. For each DCT scan, the acquired 81 transmitted diffraction projections covering 320° rotation were segmented to generate binarized images that contain only diffraction spots. This spot segmentation was done by first a background correction by rolling median subtraction, then a Laplacian of Gaussian based segmentation. More details can be found elsewhere [22].

A minimum completeness of 0.45 was set and 11 hkl families, i.e. {224}, {213}, {123}, {203}, {202}, {022}, {201}, {021}, {113}, {111} and {103}, were used for the grain reconstruction. A first grain reconstruction was performed using the raw geometry information, i.e. L_{sd} = 162 mm and zero detector offsets and tilts. Then, geometry fitting was carried out by comparing the forward projected spots from the first grain map and experimental spots to refine the geometric parameters of L_{sd}, detector offsets and tilts, using a forward projection model [23].

Using the fitted geometry, three final grain maps by merging indexed regions with mis-orientations <0.25° were reconstructed for the three independent DCT scans. Notably, between each DCT scan, there was a small but non-negligible sample position change. Ultimately, these grain maps were stacked together to show a full grain map for the whole sample volume.

2.2.3. Polarized neutron tomography

The study of the internal distribution of the trapped field in the sample has been achieved via Polarized Neutron Tomography (PNT) on the imaging station, PONTO, of the Helmholtz Zentrum Berlin. The device operates with neutrons of a wavelength 3.2 Å. The incident neutron beam is spin polarized via a solid state bender that works in transmission. The polarized beam is collimated and further filtered for neutrons of undesired spin orientation by a collimating device. The collimated beam then interacts with the sample inside a closed-fridge cryostat coolable to $T = 4.0$ K. With negligible scattering from the system, the neutron spin interacts with the magnetic field along the neutron's trajectory and the final beam is analyzed by a solid state bender that works in reflection before getting to the detector.

To facilitate 3D vectorial reconstruction of the internal magnetic field distribution of the sample 4 half-pi flippers are integrated to the standard polarized neutron imaging setup, 2 directly before the sample position and 2 directly after the sample position. The flippers before the sample allow orientation of the incident neutron polarization in one of the 3 Cartesian directions for the neutrons incident on the sample. On the other hand, the flipper set after the sample allow for analysis of the resulting polarization for one of its 3 Cartesian components. These result in obtaining 3 × 3 sets of radiographies. Each set consists of 51 radiographies and the images are obtained for every 7.2° step in a 360° rotation of the sample. There is a 120 s exposure for each radiograph. Correction for dark currents on the detector and the neutron beam inhomogeneities are done using dark-field and flat field images each obtained with the same exposure time.

YBCO is a type II superconductor meaning that under certain circumstances an applied magnetic field is not completely expelled from the bulk of YBCO from the Meissner effect [24]. Under these conditions, in an applied magnetic field, magnetic flux exists in the material in the form of single flux quanta which interact repulsively.

On removing the externally applied field while the material remains superconducting, these flux quantum can be pinned in the material in regions where there will be a resultant gain in condensation energy. Field trapping in the superconducting sample is achieved via field cooling in a magnetic field of 0.5 mT produced by a Helmholtz coil. The field is applied in the direction perpendicular both to the neutron beam travel and the long axis of the sample as shown in Fig. 2 (x direction) before being switched to 0 mT. The value of 0.5 mT is chosen due to the phase wrapping problem [25], a particular limitation of the polarized neutron tomography technique. The system is cooled to $T = 90.5$ K below the sample transition temperature and the applied magnetic field turned off leaving only field trapped in the sample. The magnetic field trapped in the sample bulk is then reconstructed using Tensorial Algebraic Reconstruction Technique (TMART) algorithm. Details on the theory of spin precession and the TMART algorithm are explained elsewhere [26].

3. Results

3.1. Neutron diffraction contrast tomography

The grain reconstruction from the DCT data reveals that there are 47 grains in the sample. From each stacks along the z axis as divided by the experiment, we investigate a slice from the grain reconstruction. This is shown in Fig. 3 with coloured dashed lines to highlight the positions of the slices. The colour coding will be maintained through the rest of the work. The focus on the grain slices in the x-y plane is done as this plane is parallel to the direction of the applied magnetic field for the PNT experiment (x axis direction). From the blue coded slice, we can see that there are big grains in the centre with smaller grains in the periphery. The big grains in the centre of the plane seem to be quite isotropic in orientation. Looking at the red coded slice, there are also big grains in the centre of the plane. In contrast to the previous slice, the central grains seem to have a preferred orientation. There are still smaller grains

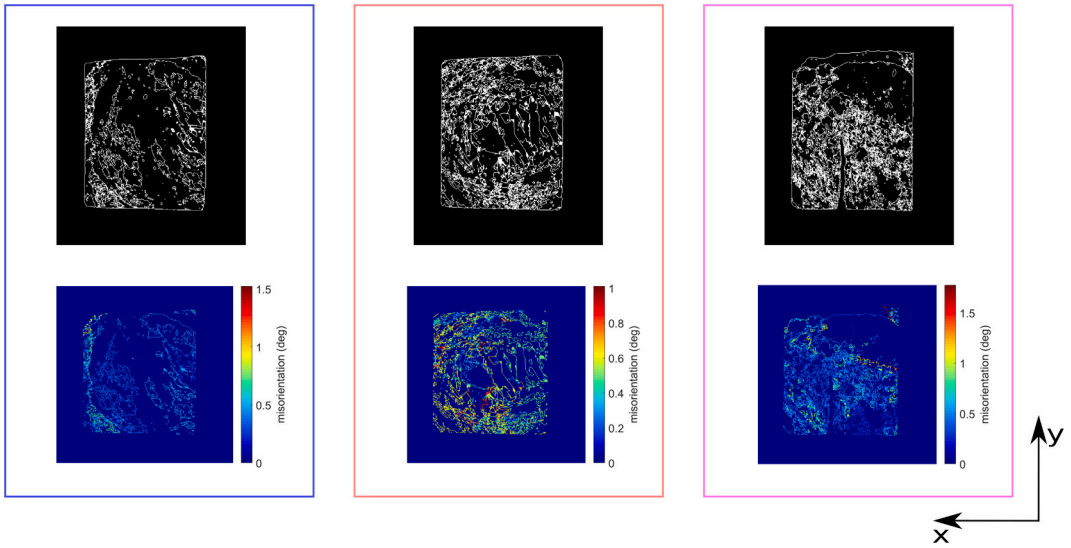

Fig. 4. Corresponding images of the grain boundaries and the grain boundary orientations for the selected slices with the same colourcoding. The sample is pseudo-single crystal with low angle grain boundaries with the highest value of θg being 1.86°.

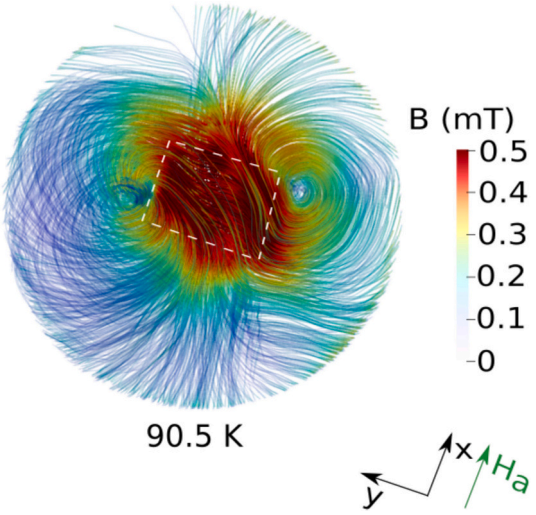

Fig. 5. Plan view of streamline visualization of the 3D reconstructed trapped vector field in $YBa_2Cu_3O_{7-\delta}$ from Polarized Neutron Tomography after field cooling to 90.5 K and switching off the field. The dashed lines indicate the sample position.

in the periphery with the orientations that seem to correspond to the boundaries at the edges. This could be a result of the hot-processing growth process. Finally, looking at the purple coded slice, there are a lot of smaller grains and there seems to be a significant directionality in the grain orientation.

Fig. 4 shows the grain boundaries and the corresponding misorientations (θ_g) for the grains from the highlighted slices. The grain boundary images are obtained via digitization of the grain reconstruction slices in order to isolate them. In the sample, the largest value of (θ_g) is 1.86° allowing the grain boundaries to be classified as low angle. In the blue coded case, there are higher values of (θ_g) at the periphery of the sample while in the red and purple coded cases, there is a relatively higher degree of misalignment of the grain boundaries with the former having a higher number of grain boundaries with higher (θ_g) values. The overall low value of (θ_g) in the material however indicates that the presence of the boundaries should not aversely affect the flow of current between the grains hence not having a significant effect on the

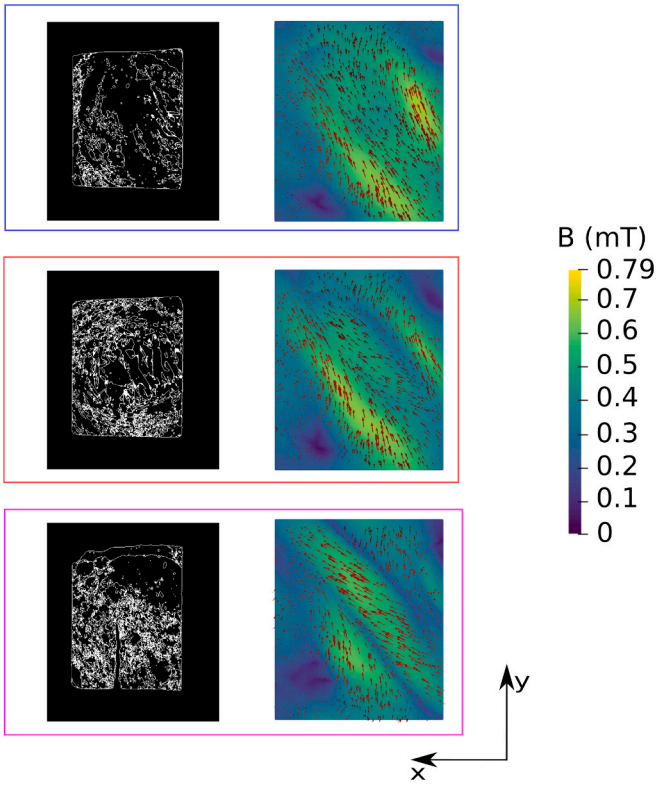

Fig. 6. Grain boundaries from the selected colour-coded slices of the grain volume reconstruction including corresponding slices of the reconstructed magnetic field with the colourmap representing the field magnitude and the red arrows representing the direction of the field. The field direction is about 45° away from applied field direction during field cooling i.e. x axis. This discrepancy is likely a result of the grain orientation. (For interpretation of the references to colour in this figure legend, the reader is referred to the web version of this article.)

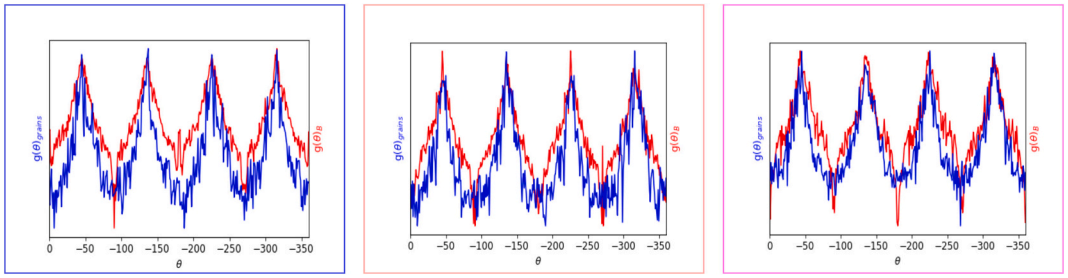

Fig. 7. Power Spectral Density from the selected slices for the field magnitude $g(\theta)_B$ and the grain boundaries $g(\theta)_{grains}$. The alignment of peaks at identical positions for both PSDs in each slice serves as an indicator suggesting a potential correlation between the grain boundaries and the magnitude of trapped field in the sample.

intergrain J_C [27].

3.2. Polarized neutron tomography

In Fig. 5, the vector field streamlines obtained from the reconstructed polarized neutron tomography data are shown. The perspective of the result is from the plan view of the material. It is observable that the mean direction of the trapped flux is different from the direction of the applied field. Investigating how the grain/grain boundary orientation correlates to the trapped field vector could be insightful to elucidating the origins of this discrepancy.

Adhering to the previously established method, the colour-coded sample slice positions are used to explore potential correlations between grain properties and the trapped field. Fig. 6 shows corresponding slice for the field reconstruction where the colourmap corresponds to the magnitude of the field while the arrows indicate the direction of the field. In addition, the arrow sizes are scaled with the magnitude of the field in those regions. For the three cases, there appears to be a mean direction of trapped field that is different from the direction of the applied field. Comparing the image of the grain boundary orientation with that of the magnetic field direction, there is an apparent correlation between the trapped field direction and the orientation of the grains/grain boundaries. The challenge remains to distinguish whether this correlation comes primarily from field in the grains or grain boundaries. This highlights the main drawback of the technique, which is the resolution of the reconstructed trapped field.

Regardless, further analysis can be done on the data to obtain more information on the relationship between flux pinning and the orientation of grains/grain boundaries. This involves the application of the fast fourier transform (FFT) and subsequent calculation of the power spectral density (PSD) from this. The FFT analysis is done on the grain boundary image and also performed directly on the field magnitude slices using the ImageJ software. The PSD is essentially obtaining the azimuthal sum of the squared FFT image. Fig. 7 shows the result from the analysis through the comparison of the PSD of both the grain boundary image and the image of the trapped field magnitude. The grains and field magnitude PSD are plotted over each other showing that the peaks in both spectra exist in the same angular locations. This is a clear indication of a correlation between the field and the grain boundaries. It is important to clarify that the correlation is only with the field magnitude. This suggests a preference for the flux trapping in the grain boundaries. Combining this with the aforementioned apparent directional correlation, an inference can be made that in the case of the study, upon field cooling, field is preferentially trapped along the grain boundaries in addition to the grain boundaries determining the anisotropy of the trapped flux.

4. Conclusion

Facilitated by tomography techniques, we have taken advantage of the neutron's properties to investigate the the effects of grain/grain boundary orientation on the trapping of flux in pseudo-single crystal YBCO. We have found that there is a directional dependence of the flux pinning mechanism on the grain orientation. Limited by the resolution of the polarized neutron tomography technique, it is a challenge to distinguish whether this dependence is a result of the grains or the grain boundaries. However, based on further analysis, an inference can be made that there is preferential flux pinning along the grain boundaries of the material from the particular conditions of this experiment.

CRediT authorship contribution statement

U.K. Oji: Supervision, Resources, Methodology. **H. Fang:** Writing – review & editing, Visualization, Software, Formal analysis. **W. Ludwig:** Supervision, Resources, Methodology. **P. Lhuisser:** Supervision, Resources, Methodology. **Stavros Samothrakitis:** Writing – review & editing, Methodology, Investigation. **Camilla Buhl Larsen:** Writing – review & editing, Methodology, Investigation. **A. Hilger:** Visualization, Software, Methodology, Investigation, Formal analysis. **I. Manke:** Supervision, Resources, Methodology, Conceptualization. **M. Tovar:** Resources. **R. Cubitt:** Writing – review & editing, Supervision, Methodology, Investigation. **N. Kardjilov:** Writing – review & editing, Validation, Supervision, Resources, Project administration, Methodology, Investigation, Conceptualization.

Declaration of competing interest

The authors declare that they have no known competing financial interests or personal relationships that could have appeared to influence the work reported in this paper.

Data availability

Data will be made available on request.

Acknowledgements

The neutron tomography experiments were performed at the Helmholtz Zentrum Berlin. This work was jointly funded by Institut Laue Langevin and the Helmholtz Zentrum Berlin. We thank the Neel Institute Magnetometry Platform (PMag) for access to the magnetometry facilities. The authors wish to acknoweldge the technical contributions of M. Krzyzagorski and M. Osenberg from the Helmholtz Zentrum Berlin.

References

[1] D.C. van der Laan, M. Dhallé, L.M. Naveira, H.J.N. van Eck, A. Metz, J. Schwartz, M.W. Davidson, B. ten Haken, H.H.J. ten Kate, Direct experimental analysis of the relation between the grain structure and the distribution of critical current density in YBa2Cu3Ox coated conductors, Supercond. Sci. Technol. 18 (3) (2005) 299–306, https://doi.org/10.1088/0953-2048/18/3/016.

[2] C. Jooss, B. Bringmann, M.P. Delamare, H. Walter, A. Leenders, H.C. Freyhardt, Current distributions of grain boundaries in differently processed melt-textured YBa2Cu3O7, Supercond. Sci. Technol. 14 (5) (2001) 260–275, https://doi.org/10.1088/0953-2048/14/5/306.

[3] W. Lo, D.A. Cardwell, C.D. Dewhurst, H.T. Leung, J.C.L. Chow, Y.H. Shi, Controlled processing and properties of large Pt-doped Y–Ba–Cu–O pseudocrystals for electromagnetic applications, J. Mater. Res. 12 (11) (1997) 2889–2900, https://doi.org/10.1557/JMR.1997.0383.
[4] A. Koblischka-Veneva, M.R. Koblischka, K. Berger, Q. Nouailhetas, B. Douine, M. Muralidhar, M. Murakami, Comparison of Temperature and Field Dependencies of the Critical Current Densities of Bulk YBCO, MgB2, and Iron-Based Superconductors, IEEE Trans. Appl. Supercond. 29 (5) (2019) 1–5, https://doi.org/10.1109/TASC.2019.2900932.
[5] D. Dimos, P. Chaudhari, J. Mannhart, Superconducting transport properties of grain boundaries in YBa2Cu3O7 bicrystals, Phys. Rev. B 41 (7) (1990) 4038–4049, https://doi.org/10.1103/PhysRevB.41.4038.
[6] S.-W. Chan, D.M. Hwang, R. Ramesh, S.M. Sampere, L. Nazar, R. Gerhardt, P. Pruna, Study of YBa2Cu3O7-x Thin Films Grown on Single Crystal SrTiO3: Not all High Angle Grain Boundaries Destroy JC, AIP Conference Proceedings American Institute of Physics 199:1 (0094-243X), 1990.
[7] T.S. Ravi, D.M. Hwang, R. Ramesh, S.W. Chan, L. Nazar, C.Y. Chen, A. Inam, T. Venkatesan, Grain boundaries and interfaces in Y-Ba-cu-O films laser deposited on single-crystal MgO, Phys. Rev. B 42 (16) (1990) 10141–10151, https://doi.org/10.1103/PhysRevB.42.10141.
[8] S.W. Chan, Nature of grain boundaries as related to critical currents in superconducting YBa2Cu3O7-x, J. Phys. Chem. Solids 55 (12) (1994) 1415–1432, https://doi.org/10.1016/0022-3697(94)90568-1.
[9] J. Lin, J. Linek, R. Kleiner, D. Koelle, NanoSQUIDs from YBa2Cu3O7/SrTiO3 superlattices with bicrystal grain boundary Josephson junctions, Nanoscale 12 (38) (2020) 20016–20024, https://doi.org/10.1039/D0NR05446A.
[10] C.P. Foley, S.K.H. Lam, J. Du, E.E. Mitchell, J. Lazar, W. Purches, S. Keenan, M. Bick, D. Clark, K. Leslie, A grain boundary Josephson junction that supported many careers and led to applications with impact, J. Supercond. Nov. Magn. 34 (6) (2021) 1611–1619, https://doi.org/10.1007/s10948-020-05698-6.
[11] M. Tachiki, S. Takahashi, Strong vortex pinning intrinsic in high-TC oxide superconductors, Solid State Commun. 70 (3) (1989) 291–295, https://doi.org/10.1016/0038-1098(89)90330-X.
[12] M. Tachiki, S. Takahashi, Anisotropy of critical current in layered oxide superconductors, Solid State Commun. 72 (11) (1989) 1083–1086, https://doi.org/10.1016/0038-1098(89)90251-2.
[13] H. Yamasaki, I. Yamaguchi, M. Sohma, W. Kondo, H. Matsui, T. Manabe, T. Kumagai, Temperature dependence of magnetic-field angle dependent critical current density and the flux pinning in YBa2Cu3O7 thin films, Physica C 478 (2012) 19–28, https://doi.org/10.1016/j.physc.2012.03.027.
[14] A. Diaz, L. Mechin, P. Berghuis, J.E. Evetts, Evidence for Vortex pinning by dislocations in YBa2Cu3O72d low-angle grain boundaries, Phys. Rev. Lett. 80 (17) (1998).
[15] T. Horide, K. Matsumoto, Evaluation of vortex pinning across low angle grain boundary in YBa2Cu3O7 film, Appl. Phys. Lett. 101 (11) (2012) 112604, https://doi.org/10.1063/1.4752462.
[16] J.H. Durrell, M.J. Hogg, F. Kahlmann, Z.H. Barber, M.G. Blamire, J.E. Evetts, Critical current of YBa2Cu3O7-δ low-angle grain boundaries, Phys. Rev. Lett. 90 (24) (2003) 247006, https://doi.org/10.1103/PhysRevLett.90.247006.
[17] I. Kotsis, M. Enisz, T. Korim, Hot pressing of YBCO-type superconductors, Superlattice. Microst. 21 (3) (1997) 435–446, https://doi.org/10.1006/spmi.1996.0414.
[18] R. Liang, D. Bonn, W. Hardy, Growth of high quality YBCO single crystals using BaZrO3 crucibles, Phys. C Superconduct. 304 (1–2) (1998) 105–111, https://doi.org/10.1016/S0921-4534(98)00275-5.
[19] S. Samothrakitis, C.B. Larsen, A. Kaestner, E. Polatidis, J. Čapek, J. Hovind, A. Fazan, J. Allibon, M. Busi, S. Schmidt, J. Kopeček, M. Strobl, The FALCON double-detector Laue diffractometer add-on for grain mapping at POLDI, J. Appl. Crystallogr. 56 (6) (2023) 1792–1801, https://doi.org/10.1107/S1600576723009640.
[20] H. Fang, W. Ludwig, P. Lhuissier, Reconstruction algorithms for grain mapping by laboratory X-ray diffraction contrast tomography, J. Appl. Crystallogr. 55 (6) (2022) 1652–1663, https://doi.org/10.1107/S1600576722010214.
[21] H. Fang, GrainRecon, Available at, https://gricad-gitlab.univ-grenoble-alpes.fr/TomoXSIMaP/GrainRecon.
[22] H. Fang, D. Juul Jensen, Y. Zhang, Improved grain mapping by laboratory X-ray diffraction contrast tomography, IUCrJ 8 (4) (2021) 559–573, https://doi.org/10.1107/S2052252521003730.
[23] H. Fang, D. Juul Jensen, Y. Zhang, A flexible and standalone forward simulation model for laboratory X-ray diffraction contrast tomography, Acta Crystallogr. Sect. A Found. Adv. 76 (6) (2020) 652–663, https://doi.org/10.1107/S2053273320010852.
[24] R.P. Huebener, Magnetic Flux Structures in Superconductors vol. 6, Springer, Berlin Heidelberg, Berlin, Heidelberg, 2001, https://doi.org/10.1007/978-3-662-08446-5 of Springer Series in SOLID-STATE SCIENCES,.
[25] M. Strobl, H. Heimonen, S. Schmidt, M. Sales, N. Kardjilov, A. Hilger, I. Manke, T. Shinohara, J. Valsecchi, Polarization measurements in neutron imaging, J. Phys. D. Appl. Phys. 52 (12) (2019) 123001, https://doi.org/10.1088/1361-6463/aafa5e.
[26] A. Hilger, I. Manke, N. Kardjilov, M. Osenberg, H. Markötter, J. Banhart, Tensorial neutron tomography of three-dimensional magnetic vector fields in bulk materials, Nat. Commun. 9 (1) (2018) 4023, https://doi.org/10.1038/s41467-018-06593-4.
[27] D.M. Feldmann, T.G. Holesinger, R. Feenstra, D.C. Larbalestier, A review of the influence of grain boundary geometry on the electromagnetic properties of polycrystalline YBa2Cu3O7-x films, J. Am. Ceram. Soc. 91 (6) (2008) 1869–1882, https://doi.org/10.1111/j.1551-2916.2008.02273.x.